Journal of Southeast University (English Edition) Vol. 39, No. 4, pp. 350 - 360 Dec. 2023 ISSN 1003—7985

Floor response spectra for seismic performance tests of nonstructural components

Shang Qingxue[1,2,3] Li Haiyang[2,3] Li Jichao[2,3] Wang Tao[2,3]

([1]China Earthquake Disaster Prevention Center, Beijing 100029, China)

([2]Key Laboratory of Earthquake Engineering and Engineering Vibration, Institute of Engineering Mechanics, China Earthquake Administration, Harbin 150080, China)

([3]Key Laboratory of Earthquake Disaster Mitigation of Ministry of Emergency Management, Harbin 150080, China)

Abstract: To determine the inputs of shaking table tests for acceleration-sensitive nonstructural components (NSCs), floor acceleration response spectra (FRS) for shaking table tests on NSCs were developed. Shaking table tests were conducted on floating-type medical infusion racks to verify the applicability of the proposed FRS. Nonlinear time-history analyses of standard frame structures under different earthquake intensities were conducted to determine the dynamic amplification factors (DAFs) of NSCs. Furthermore, FRS for seismic performance tests of NSCs were developed based on this analysis results. Shaking table tests for medical infusion racks were conducted using the proposed FRS and those for NSC tests. Seismic fragility curves under different earthquake inputs were generated based on the shaking table test results. The proposed response spectrum comprises short period, linear increase, plateau, and decrease segments. The DAF for the plateau segment should be 3.0. The test results indicate that the medical infusion racks exhibit a 50% probability of reaching or exceeding a residual displacement of 500 mm under the acceleration input of 0.307 4g. Therefore, the proposed FRS can be used for determining the table inputs for shaking table tests for performing the seismic performance tests of NSCs, facilitating seismic performance research on acceleration-sensitive NSCs.

Key words: nonstructural component; floor response spectra; shaking table test; seismic performance test; seismic fragility curve

DOI: 10.3969/j.issn.1003-7985.2023.04.004

In the seismic design codes of China, nonstructural components (NSCs) mainly include durable architectural nonstructural elements and electromechanical equipment supported by the main structure[1]. Statistical results of Taghavi and Miranda[2] show that the construction cost of NSCs accounts for a large portion of the total investment in buildings. For modern public buildings, such as office buildings, hotels, and hospitals, the investment for NSCs reaches 82%, 87%, and 92% of the total cost, respectively. The results of previous seismic damage surveys have shown that damages incurred to NSCs are much more costly than those incurred to structural components. In addition, casualties and loss of building functionality have occurred because of damages to NSCs. The statistical results of the 2013 Lushan earthquake showed that numerous medical equipment were damaged in local hospitals, and many hospitals encountered a shortage of medical equipment and medicine storage space, severely affecting their emergency rescue functionality[3].

Numerical modeling[4-5], seismic design[6-7], and seismic test methods[8-9] for structural systems and components have been developed in past decades. However, previous seismic damage survey results remind us that attention should be paid to research on the NSC damage mechanism in buildings[10-11], particularly for important or densely populated buildings, such as hospitals and schools. Studying the damage to NSCs and exploring methods for reducing their damages are necessary to avoid substantial economic losses caused by seismic damage, severe consequences of the building functionality loss, and the social impact of post-earthquake suspension.

NSCs can be classified into displacement-, acceleration-, and hybrid-sensitive types based on their response characteristics. Among these types, the failure of displacement-sensitive NSCs is primarily controlled by the interstory drift of the supporting structure. The seismic performance tests of displacement-sensitive NSCs mostly adopt pseudo-static tests. The failure of hybrid-sensitive NSCs is closely related to interstory drift and floor acceleration. The failure of acceleration-sensitive NSCs is mainly controlled by the floor acceleration, and the seismic performance evaluation often uses dynamic loading or shaking table tests[12-13]. For shaking table tests for NSC seismic performance evaluation, determining the corresponding floor acceleration response spectra (FRS) based

Received 2023-09-11, **Revised** 2023-10-25.

Biographies: Shang Qingxue (1993—), male, doctor, senior engineer; Wang Tao (corresponding author), male, doctor, researcher, wangtao@iem.ac.cn.

Foundation items: The National Key Research and Development Program of China (No. 2022YFC3803003), the National Science Foundation for Distinguished Young Scholars (No. 52125806), the National Natural Science Foundation of China (No. 52208483).

Citation: Shang Qingxue, Li Haiyang, Li Jichao, et al. Floor response spectra for seismic performance tests of nonstructural components[J]. Journal of Southeast University (English Edition), 2023, 39(4): 350 - 360. DOI: 10.3969/j.issn.1003-7985.2023.04.004.

on the test requirements and generating suitable artificial acceleration time histories are often necessary. The commonly used FRS for tests of NSCs include ICC-ES AC156[14] and IEEE Std 693-2005[15]. In China, GB 50994—2014[16] for electrical equipment and YD 5083—2005[17] for telecommunication equipment are widely used. Di Sarno et al.[18] generated artificial accelerograms based on ICC-ES AC156[14] for the seismic performance evaluation of medical cabinets and established the corresponding fragility models. Kuo et al.[19] investigated the dynamic response of medical cabinets using sine excitation. Huang et al.[20] examined the dynamic response of vases based on ICC-ES AC156[14]. Shang[21] studied the dynamic response and fragility of suspended pipelines based on ICC-ES AC156[14]. Bai et al.[22] investigated the seismic performance of porcelain column-type electrical equipment based on IEEE Std 693-2005[15]. Although many research studies have examined seismic performance tests of NSCs based on FRS, a universal FRS for these tests and experimental research on NSCs are still lacking in China. This paper focused on the problem of insufficient consideration of long period components in existing FRS for seismic performance tests of NSCs. Based on the abovementioned research background, this paper conducts nonlinear time-history analysis (NTHA) of four-, eight-, and twelve-story reinforced concrete (RC) frame structures to obtain the floor absolute acceleration response time history of each floor of the main structure under different ground motion intensities, calculate the FRS and peak floor acceleration, and generate the dynamic amplification factor (DAF) of NSCs. Based on the analysis results, a general FRS suitable for seismic performance tests of NSCs is established. Shaking table tests were conducted on medical infusion racks to investigate the seismic responses. A comparison with the existing FRS reveals the effectiveness and usability of the developed FRS.

1 Floor Response Spectra for Tests of Nonstructural Components

1.1 Supporting structure information

Considering that the most widely used buildings in China adopt frame structures, this study adopts frame structures for NTHA to determine the DAF distribution of NSCs. Based on the current design codes in China[1], four-, eight-, and twelve-story strong column and weak beam RC frame structures were designed. The plan and elevation layouts of the prototype frame structures are shown in Fig. 1, where z is the height of the structure with respect to grade at the point of attachment of the component, h is the structure roof height relative to the base elevation. Finite element models of the structures

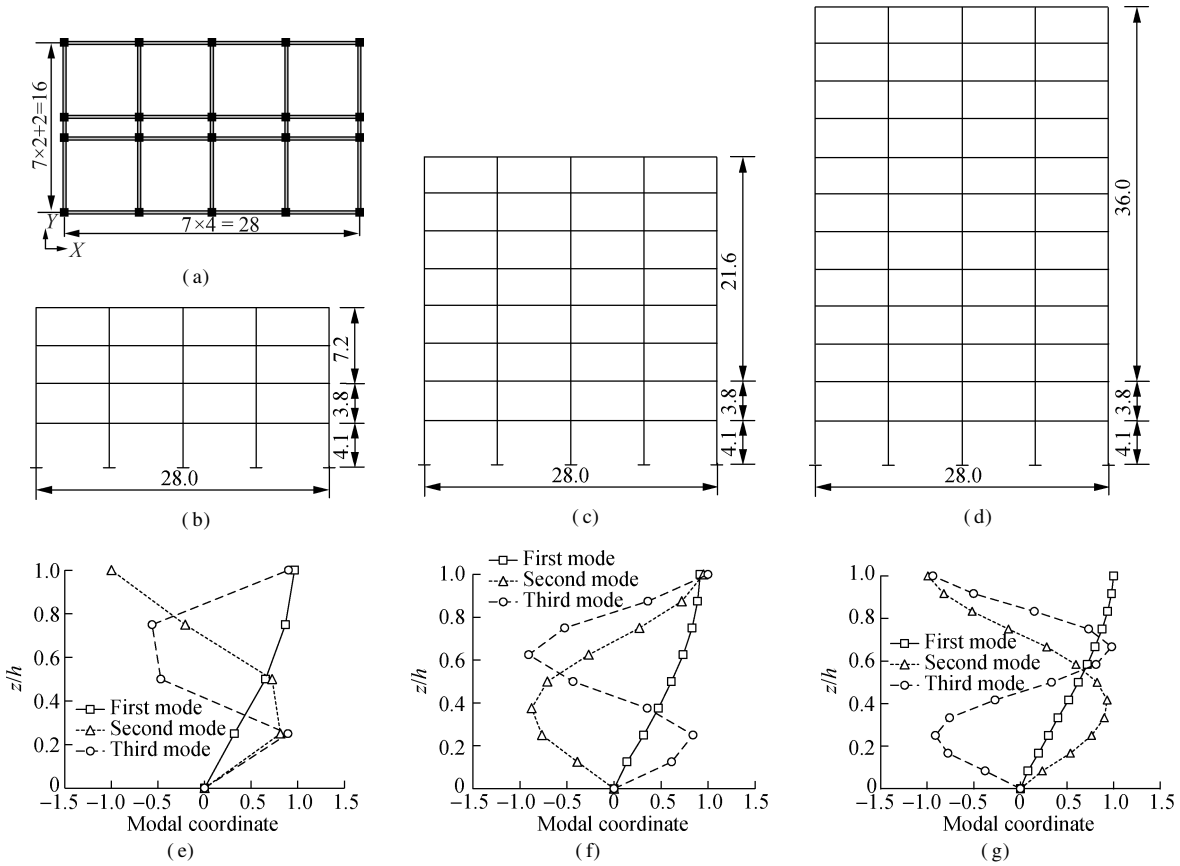

Fig. 1 Supporting structure. (a) Layout of the prototype frames (unit: m); (b) Lateral view of the four-story frame (unit: m); (c) Lateral view of the eight-story frame (unit: m); (d) Lateral view of the twelve-story frame (unit: m); (e) Modal shape of the four-story frame; (f) Modal shape of the eight-story frame; (g) Modal shape of the twelve-story frame

were developed based on OpenSees software. Because the three-dimensional finite element model using fiber sections contains many elements and requires a long calculation time, only one frame, which is in the *X*-direction of the structure, was considered. The three-dimensional model was simplified into a two-dimensional fishbone model for enhancing the NTHA calculation efficiency. As a compromise between detailed finite element models and simplified models, the fishbone model provides a rational way to explicitly include the effect of column-to-beam strength and stiffness ratios for simulating the dynamic responses of moment frames at a relatively low computational cost compared with detailed finite element models. When an *N*-span plane frame is condensed into a fishbone model, the number of degrees of freedom of the problem is approximately reduced to $1/N$ of its original size. The corresponding reduction in computational cost is particularly attractive when NTHA needs to repeat calculations with multiple ground motions under different intensities[23-24]. The specific design information, modeling information, and verification results of the finite element models are omitted here because of space limitations but can be found in Refs. [23 − 24]. The modal periods and mass distributions of the structures are shown in Table 1. For NTHA, a set of 20 ground motions, 15 recorded and 5 artificial motions, was used. The 15 recorded ground motions were selected from the PEER-NGA Database, and their specific information was reported in Ref. [10].

Table 1 Modal period and mass

Structure	Mode	Modal period/s	Modal mass/t	Mass participation coefficient/%
Four-story	1	0.656	490.4	88.16
	2	0.206	50.1	9.02
	3	0.123	13.9	2.49
Eight-story	1	1.068	1 010.2	83.60
	2	0.355	112.1	9.28
	3	0.202	38.3	3.17
Twelve-story	1	1.656	1 458.5	79.63
	2	0.574	294.4	16.07
	3	0.340	45.1	2.46

The artificial ground motions were generated based on the design spectra specified in the Chinese design code[1].

1.2 Floor response spectra calculation results

The procedure for calculating the FRS based on NTHA is shown in Fig. 2, where $\ddot{u}_g(t)$ represents the ground motion acceleration, $\ddot{u}_n(t)$ represents the floor acceleration response of the *n*-th floor. Determining the design response spectra acceleration (S_a) of the supporting structure based on the site conditions and selecting appropriate ground motions as inputs are crucial for NTHA. Further, the finite element model of the structure is developed, and NTHA is conducted to obtain the absolute acceleration response for each floor. The floor acceleration response is then used for calculating the corresponding FRS. Additionally, NTHA provides the floor acceleration amplification factor (FAA), which is the ratio of the peak floor acceleration (PFA) to the peak ground acceleration (PGA). The FAA reflects the amplification effect for each floor on the ground acceleration[25]. Because the focus of this study is DAF, the analysis results of FAA will not be discussed here but can be found in Refs. [26 − 27]. In addition, the authors have conducted a detailed state-of-the-art review of recent studies on FRS[27].

In this study, the structure-nonstructure decoupling method is adopted for the FRS calculation, indicating that only NSCs with much smaller mass relative to the overall structural mass (e.g., $<0.1\%$ of the overall structural mass, as suggested by Toro et al.[28]) are considered, and the interaction between the structure and NSCs is neglected. The damping ratio of NSCs in this study is set to 5%, the most commonly used value for NSCs[29]. The DAF of NSCs is defined as the ratio of the FRS value to PFA, reflecting the amplification effect of NSCs on floor acceleration response.

The NTHA results of the DAF at the top floor of the four-, eight-, and twelve-story structures under different ground motion intensities (PGAs of $0.07g$, $0.20g$, and $0.40g$) are shown in Fig. 3, where β represents the dynamic amplification factor. Generally, the FRS or

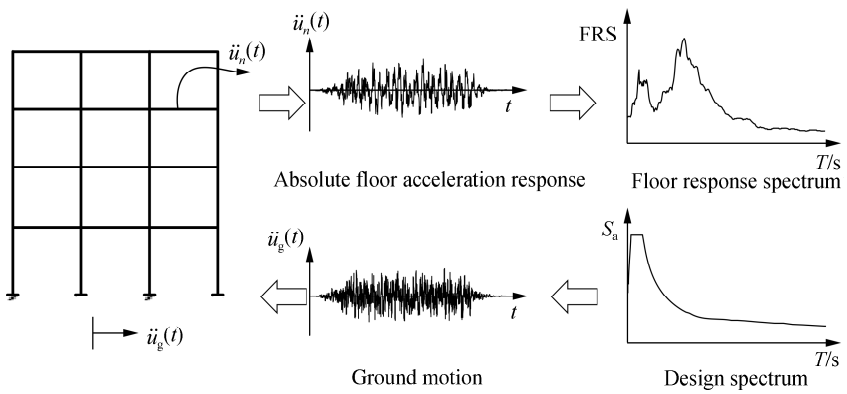

Fig. 2 Procedure for generating the floor response spectra

DAF spectrum has two to three peak points, and the periods of these peak points are identical to the natural periods of the structures in the same horizontal vibration direction. These peak points are caused by the resonance effect between the structure and NSCs. Fig. 3 also shows that the FRS obtained from different ground motions have a certain discreteness. The peak points of the FRS gradually shift toward longer periods, forming a platform effect with increasing ground motion intensity. This result is mainly due to the elongation of each modal period when the structure enters the nonlinear deformation stage and dissipates seismic energy. The platform effect is most pronounced for the first modal period and less pronounced for higher modes. In addition, the period of the NSC corresponding to the highest peak point of DAF does not always fall near the first natural period of the structure. For example, for the twelve-story structure, the highest peak point of DAF is near the second natural period of the structure. Furthermore, the NSCs have a negligible resonance effect with the third and higher modes of the structure.

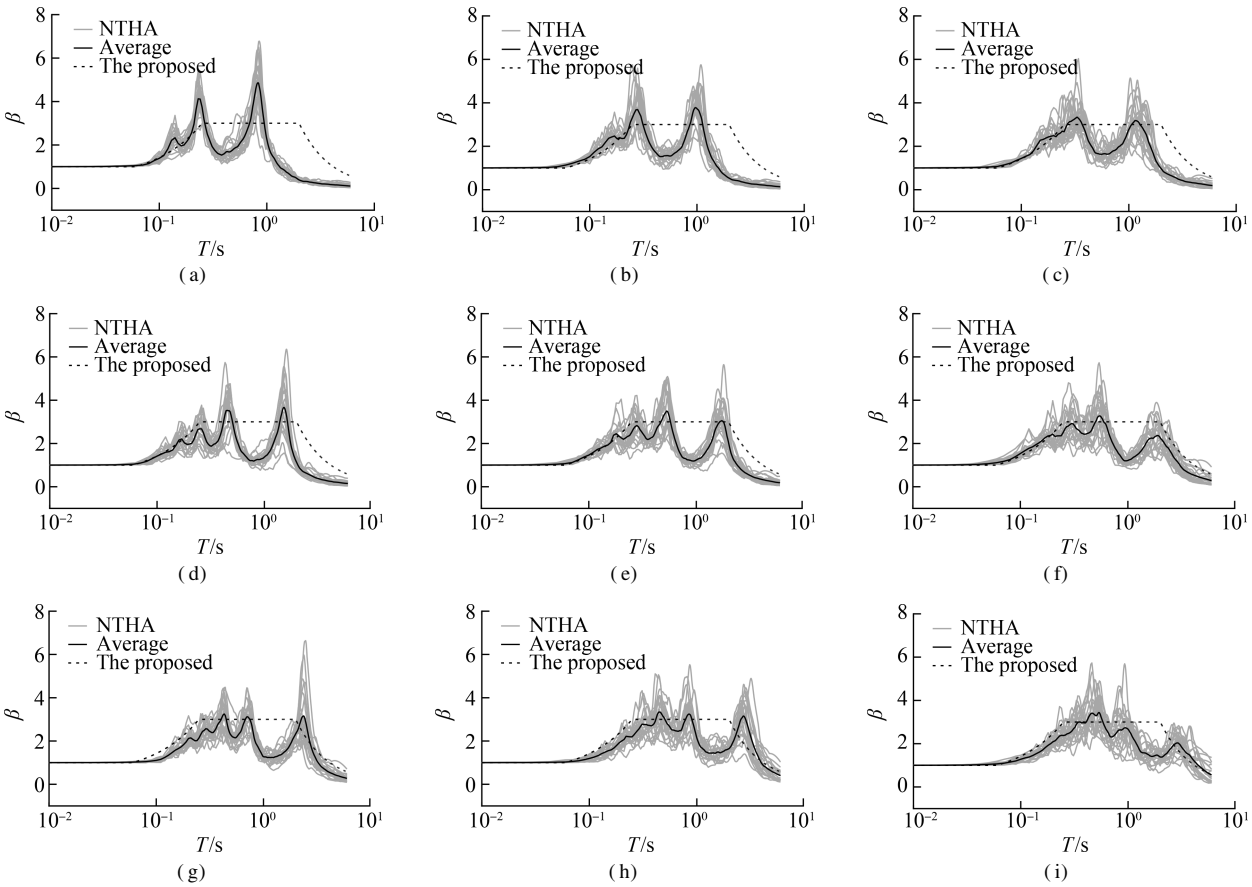

Fig. 3 Dynamic amplification factors of nonstructural components. (a) Four-story frame under 0.07g inputs; (b) Four-story frame under 0.20g inputs; (c) Four-story frame under 0.40g inputs; (d) Eight-story frame under 0.07g inputs; (e) Eight-story frame under 0.20g inputs; (f) Eight-story frame under 0.40g inputs; (g) Twelve-story frame under 0.07g inputs; (h) Twelve-story frame under 0.20g inputs; (i) Twelve-story frame under 0.40g inputs

The globally used seismic design codes for the DAF of NSCs are shown in Fig. 4. Overall, the codes in various countries adopt simplified definitions for quantifying DAF, and most definitions consider the influence of NSC stiffness. According to the Chinese code[1,30-31], the DAF values can be taken as 2.0 for prefabricated building components, cantilever components, and any equipment with support points below the centroid, while the value is 1.0 for other cases. The American code (ASCE/SEI 7-16)[32] stipulates that DAF should be 1.0 for rigid components (NSCs with a natural period (T) smaller than 0.06 s) and 2.5 for flexible components (NSCs with a natural period longer than 0.06 s). The New Zealand code (NZS 1170.5: 2004)[33] divides DAF distribution into three segments based on the natural period of NSCs; with increasing T, DAF decreases monotonically, as defined in Eq. (1). The Chinese design guideline CECS 160—2004[34] and American FEMA P-750[35] further consider the influence of the first natural period (T_1) of the supporting structure on DAF. These two codes divide DAFs into five segments with linear distribution, as defined in Eq. (2). The European code (BS EN 1998-1: 2004)[36] considers the influence of T_1 and height z of NSCs, as shown in Eq. (3). The relationships between the DAF of NSCs and their natural periods for the existing seismic design codes are rough. According to the calculation results in Fig. 3,

the DAF values of NSCs at multiple periods are up to 3- to 7-fold larger than those prescribed in various codes. Moreover, provisions in the abovementioned codes are mainly used for calculating the equivalent lateral forces in NSC seismic design and, hence, are difficult to apply directly to NSC seismic tests[27].

$$\beta=\begin{cases}2.0 & 0\leqslant T\leqslant 0.75\\ 2(1.75-T) & 0.75<T<1.5\\ 0.5 & T\geqslant 1.5\end{cases} \tag{1}$$

$$\beta=\begin{cases}1.0 & 0\leqslant \dfrac{T}{T_1}\leqslant 0.5\\ 7.5\dfrac{T}{T_1}-2.75 & 0.5<\dfrac{T}{T_1}\leqslant 0.7\\ 2.5 & 0.7<\dfrac{T}{T_1}\leqslant 1.4\\ -2.5\dfrac{T}{T_1}+6.0 & 1.4<\dfrac{T}{T_1}\leqslant 2.0\\ 1.0 & \dfrac{T}{T_1}>2.0\end{cases} \tag{2}$$

$$\beta=\left[\frac{3(1+z/h)}{1+(1-T/T_1)^2}-0.5\right]\Big/\left[\frac{3(1+z/h)}{2}-0.5\right] \tag{3}$$

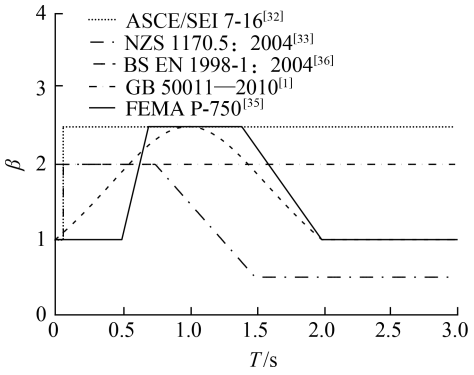

Fig. 4 Dynamic amplification factors in different design codes

1.3 Proposed floor response spectra

Seismic performance evaluation of NSCs is often conducted without knowing the specific installation location of NSCs in the supporting structure and the dynamic characteristics of NSCs. Therefore, the DAF for NSCs is divided into four segments in this study, i.e., a short period segment (0-0.06 s), a linear increase segment (0.06-0.25 s), a plateau segment (0.25-2.0 s), and a decrease segment (after 2.0 s). In the plateau segment, the DAF for NSCs is suggested to be 3.0, as shown in Eq. (4) and Fig. 3. Notably, the average curves in Fig. 3 and Fig. 5 represent the arithmetic mean values of DAF analysis results under the 20 ground motions. The proposed amplification factor in Eq. (4) almost envelopes the average curves of NTHA results. Although the peak DAF points corresponding to the natural periods of the supporting structures are slightly larger than the plateau segment value (3.0), this envelope result is acceptable because a larger value than 3.0 will be difficult to reproduce by the shaking tables in the laboratory.

$$\beta=\begin{cases}1.0 & 0\leqslant T\leqslant 0.06\\ 10.53T+0.37 & 0.06<T\leqslant 0.25\\ 3.0 & 0.25<T\leqslant 2.0\\ 3.0\left(\dfrac{2}{T}\right)^{1.5} & T>2.0\end{cases} \tag{4}$$

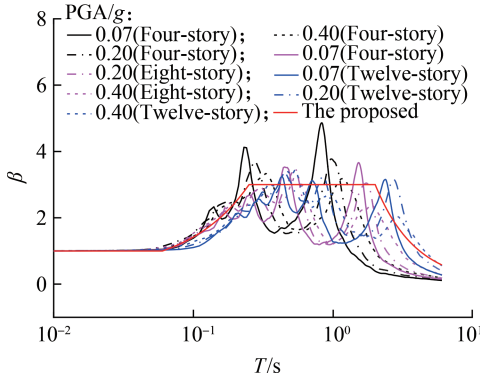

Fig. 5 Median values of the dynamic amplification factors for nonstructural components

The proposed DAF in Eq. (4) is compared with the amplification factors defined in existing codes (such as ICC-ES AC156[14], IEEE Std 693-2005[15], and YD 5083—2005[17]) and the one defined by Anajafi[37] in Fig. 6. The amplification factors defined by Anajafi[37] can be determined by Eq. (5). The DAFs specified in YD 5083—2005[17] are listed in Table 2, which shows a linear distribution between the DAFs of each frequency point in logarithmic coordinates, f is the natural frequency of nonstructural components. The short period segment of the proposed FRS refers to the relevant provisions in the current Chinese codes[1,30-31]. The DAF in the plateau segment takes the same value as that in YD 5083—2005[17] and Anajafi[37]. The starting periods of the plateau segment are set as 0.25 and 2.0 s, which include a wide range of building structural periods to consider the possible resonance effects between the structure and NSCs. However, this study only considers the NTHA results of four-, eight-, and twelve-story frame structures. Further

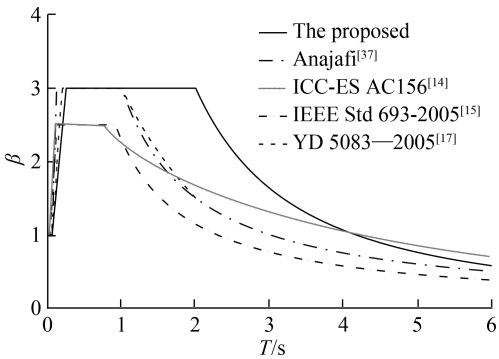

Fig. 6 Comparison of the dynamic amplification factors of nonstructural components

research and validation are needed for frame structures with different numbers of stories and other structural systems, e. g., masonry structures and shear wall structures.

$$2\beta = \begin{cases} 2.0 & 0 \leqslant T \leqslant 0.06 \\ 66.7T - 2.0 & 0.06 < T \leqslant 0.11 \\ 6.0 & 0.11 < T \leqslant 1.0 \\ \dfrac{6}{T} & T > 1.0 \end{cases} \quad (5)$$

Table 2 Dynamic amplification factors defined in YD 5083—2005[17]

f/Hz	0.5	1.0	5.0	10.0	20.0	50.0
β	1.5	3.0	3.0	1.5	1.0	1.0

2 Application in Shaking Table Tests of Nonstructural Components

2.1 Input motion

In shaking table tests, the artificial time histories generated based on the proposed FRS, ICC-ES AC156[14] and Anajafi[37] were adopted, and the responses will be compared. The corresponding acceleration time histories and response spectra are shown in Fig. 7. Unidirectional loading was conducted for different amplitudes of PFA, i. e., 0.05g, 0.07g, 0.10g, 0.14g, and 0.20g. The three motions will be individually used as shaking table inputs for each PFA value.

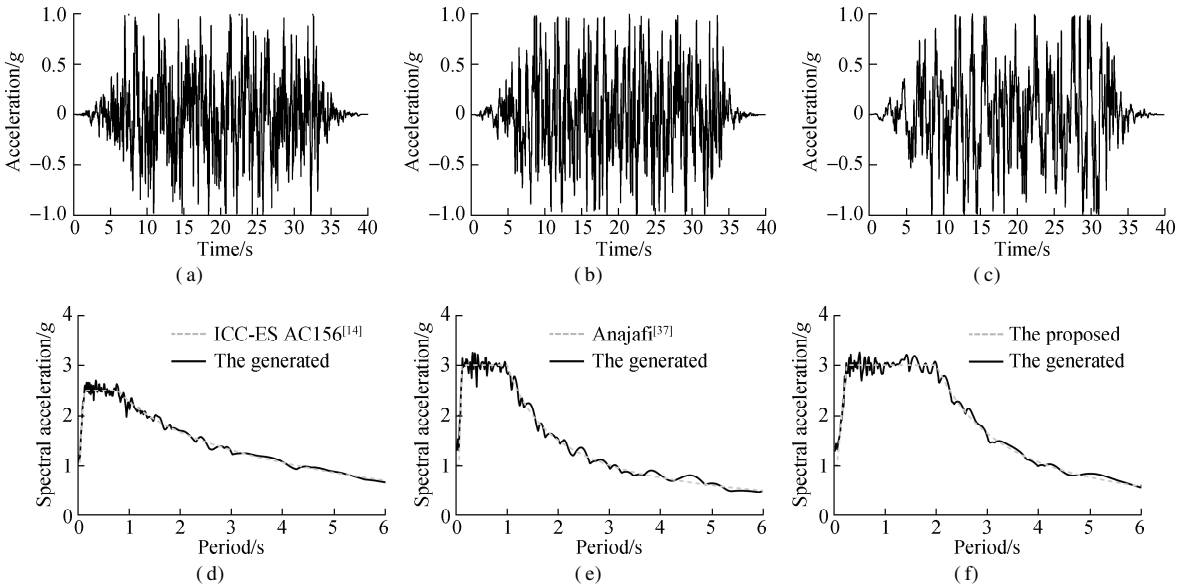

Fig. 7 Input for shaking table tests. (a) Acceleration time history of ICC-ES AC156[14]; (b) Acceleration time history of Anajafi[37]; (c) Acceleration time history of the proposed spectra; (d) Response spectra of ICC-ES AC156[14]; (e) Response spectra of Anajafi[37]; (f) Response spectra of the proposed spectra

2.2 Test setup

Floating-type medical infusion racks were selected as specimens in this study. Floating racks might fly off from the shaking table during loading; hence, they were placed in a one-story, one-span steel frame room, as shown in Fig. 8. The frame had a plan dimension of 4.35 m × 4.35 m, a column spacing of 4.2 m, a story height of 2.63 m, and one side of the exterior wall had a 1.2 m wide and 2.1 m high door. The structure was not topped, and only the bottom floor had a floor slab to provide ground finishing for the floating-type equipment. The test adopted unidirectional loading, and the arrows in Fig. 8 indicate the loading direction. Notably, the tested infusion racks are insensitive to the loading direction as they are supported by five wheels that allow the infusion racks to roll freely in different directions. To avoid possible collisions between different infusion racks, they were arranged as shown in Fig. 8 to ensure sufficient distance between

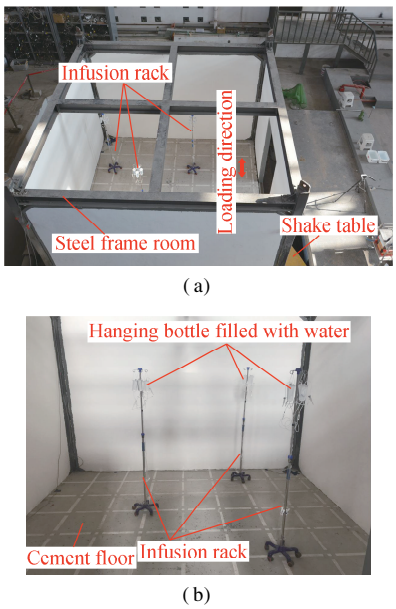

Fig. 8 Layout of medical infusion racks. (a) Top view; (b) Front view

adjacent infusion racks. Three infusion racks were installed on the cement floor, and each rack had four hanging bottles filled with water to simulate the actual usage state. The distance between the top of each infusion rack and the ground was 1.85 m.

2.3 Probabilistic seismic fragility analysis method

In this study, probabilistic seismic fragility models (PSFMs) for NSCs under various input motions are developed based on the shaking table test data. The demand distribution of the components is obtained during the shaking table test, and regression analysis is conducted to develop probabilistic seismic demand models (PSDMs). These models will be used for describing the quantitative relationship among the demand (e.g., residual displacement, maximum displacement), and seismic intensity (e.g., PFA and PGA). A previous study has shown that the demand parameter S_D follows a power-law relationship with the seismic intensity measure (M), as shown in Eq. (6). The uncertainty in the PSDM is expressed using a lognormal distribution, and the logarithmic standard deviation $\beta_{D|M}$ can be calculated using Eq. (7)[38].

$$S_D = aM^b, \quad \ln S_D = \ln a + b\ln M \tag{6}$$

$$\beta_{D|M} \cong \sqrt{\frac{\sum_{i=1}^{N} (\ln d_i - \ln(aM^b))^2}{N-2}} \tag{7}$$

where a and b are regression parameters, N is the number of sample points, and d_i is the demand obtained under the i-th motion.

Based on the PSDM, PSFMs can be further defined as the probability of reaching or exceeding a certain damage limit state of the component, i.e., the demand (D) is larger than capacity (C) under a given motion intensity[39]. The exceedance probability can be calculated by

$$P[D \geqslant C \mid M] = \Phi\left(\frac{\ln(S_D/S_C)}{\sqrt{\beta_{D|M}^2 + \beta_C^2}}\right) = \Phi\left(\frac{\ln M - (\ln S_C - \ln a)/b}{\sqrt{\beta_{D|M}^2 + \beta_C^2}/b}\right) \tag{8}$$

$$M_{\mathrm{m}} = \exp\left(\frac{\ln S_C - \ln a}{b}\right) \tag{9}$$

$$\beta_{\mathrm{F}} = \frac{\sqrt{\beta_{D|M}^2 + \beta_C^2}}{b} \tag{10}$$

where S_C is the median capacity of the component, β_C is the logarithmic standard deviation of the component capacity, M_{m} is the median motion intensity corresponding to the damage limit state, and β_{F} is the logarithmic standard deviation corresponding to the damage limit state. β_C can be set to 0 by neglecting the uncertainty of the seismic capacity of the component.

The response of the infusion racks tested in this study is mainly characterized by rolling when the wheels are released. Pounding with other objects (such as tables, walls, and surrounding medical equipment) or patients will affect their normal use when the rolling distance reaches a certain limiting value during actual use. To compare the seismic fragility under different input motions, this study defined damage states (with $\beta_C = 0$) as situations where the residual displacement or maximum displacement of the equipment is greater than or equal to the displacement threshold values under a given PFA value.

2.4 Test results

The displacement responses, including residual displacement and maximum displacement, are widely used in seismic performance analysis of medical equipment supported on wheels/casters[40]. For possible post-earthquake reconnaissance of hospital rooms, the maximum displacement responses under earthquakes are unavailable, but the residual displacement can be observed; therefore, the residual displacement of the infusion racks was considered as the representative value of the critical response index for quantifying seismic performance. The residual displacement responses of the infusion racks under different motions, which represent the demand parameter S_D presented in Section 2.3, are shown in Table 3 and Fig. 9(a). PFA was selected as the seismic intensity measure parameter, as discussed in Section 2.3. The residual displacement responses of the infusion racks and the observations in the test show that the smallest and largest responses were obtained when using the artificial input motion based on ICC-ES AC156[14] and the proposed artificial input motion in this study, respectively.

For the proposed FRS and developed artificial time history, another two loading cases with input PFAs of 0.3g and 0.4g were loaded considering the much larger responses of tested specimens under this input motion are observed compared with ICC-ES AC156[14] and Anajafi[37] motions. The relationship between the residual displacement of the infusion racks and PFA is shown in Fig. 9(b). The seismic fragility curves under a threshold of 500 mm are shown in Fig. 9(c), consistent with the distribution pattern of the response in Table 3. Notably, 500 mm is usually the approximate distance between the infusion racks and surrounding patients or other equipment; therefore, it is selected as the displacement threshold here for fragility analysis. Under the proposed artificial input motion, the exceedance probability is much higher than that obtained under the artificial input motions based on ICC-ES AC156[14] and Anajafi[37]. Notably, because of the large variations in the residual displacement response distribution under the artificial input motion of Anajafi[37], the fitting result of PSDM is not so good, resulting in a logarithmic standard deviation of 0.896 6. This fragility

Table 3 Infusion rack response

Input motion	Input PFA/g	Residual displacement/mm			Observed response
		Model 1	Model 2	Model 3	
ICC-ES AC156[14]	0.05				Bottles wobbled slightly
	0.07				Bottles wobbled and the infusion support rocked
	0.10	30			Bottles wobbled and the infusion support rocked
	0.14	20	20	30	Bottles wobbled and the infusion support rocked
	0.20	180	46	40	Bottles wobbled and the infusion support rocked
Anajafi[37]	0.05				Bottles wobbled slightly
	0.07				Bottles wobbled and the infusion support rocked
	0.10	50			Bottles wobbled and the infusion support rocked
	0.14	100	25	22	Bottles wobbled and the infusion support rocked
	0.20	255	61	40	Bottles wobbled and the infusion support rocked
The proposed	0.05				Bottles wobbled heavily
	0.07				Bottles wobbled heavily and the infusion support rocked
	0.10	60	40	10	Bottles wobbled heavily and the infusion support rocked
	0.14	80	30	20	The infusion support tended to overturn
	0.20	201	89	54	Specimen 3 almost overturned

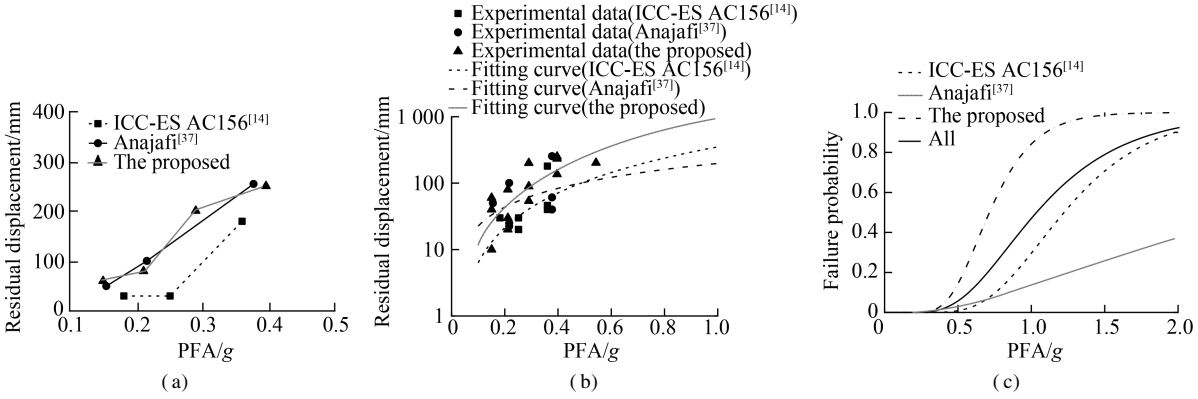

Fig. 9 Residual displacement and seismic fragility curves of infusion racks. (a) Residual displacement distribution; (b) Fitting results; (c) Seismic fragility curves of infusion supports

model is less applicable for seismic performance assessment. If the data from three different input motions could not be distinguished for probabilistic seismic demand and fragility analyses, the seismic fragility curve will be obtained as the gray solid line in Fig. 9 ("All" represents the test results under different input motions), indicating that the curves obtained under artificial input motions of ICC-ES AC156[14] and Anajafi[37] substantially underestimate the damage exceedance probability. The fragility model based on the proposed artificial input motion is relatively conservative and can satisfy the conservative requirements of NSC seismic performance tests. The corresponding parameters of PSFMs are listed in Table 4. Notably, M_m and β values are calculated for a threshold of 500 mm. The results indicate that the medical infusion racks exhibit a 50% probability of reaching or exceeding a residual displacement of 500 mm under 0.304 7g inputs when the proposed FRS are adopted for determining the shaking table input. In addition, the seismic fragility curves of infusion racks considering different displacement thresholds can be developed based on the probabilistic seismic fragility analysis results, as shown in Fig. 10.

3 Conclusions

1) The absolute acceleration response, response spectrum, and DAFs for NSCs under various ground motion intensities are calculated based on the NTHA of four-, eight-, and twelve-story frame structures. FRS for evaluating the seismic performance of acceleration-sensitive NSCs using shaking table tests are developed based on the results of these time-history analyses.

2) The suggested DAF spectra for NSCs are composed of the short period (0-0.06 s), linear increase (0.06-0.25 s), plateau (0.25-2.0 s), and decrease segments

Table 4 Parameters of probabilistic seismic demand and probabilistic seismic fragility models

Input motion	ln$a$	b	N	$\beta_{D\mid M}$	M_m/g	β_F
ICC-ES AC156[14]	5.863 4	1.744 6	7	0.654 5	0.486 2	0.375 2
Anajafi[37]	5.288 7	0.942 5	7	0.845 0	0.484 2	0.896 6
The proposed	6.856 1	1.908 2	13	0.639 7	0.307 4	0.335 2

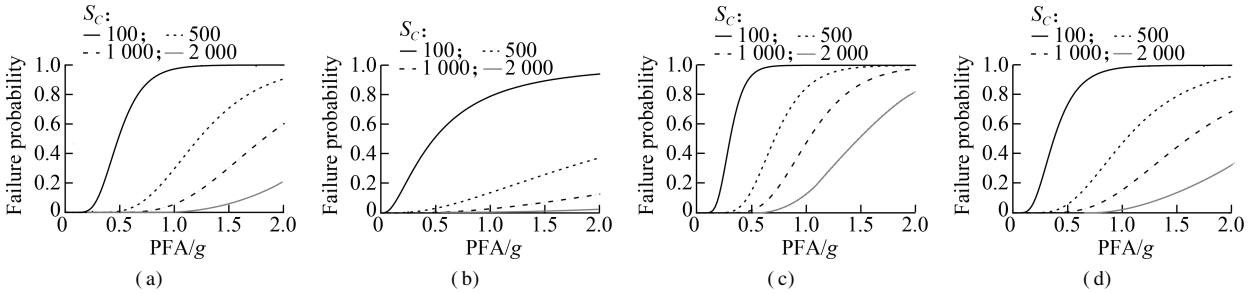

Fig. 10 Seismic fragility curves of infusion racks considering different displacement thresholds. (a) ICC-ES AC156[14]; (b) Anajafi[37]; (c) The proposed; (d) All

(after 2.0 s). In the plateau segment, the amplification factor for NSCs is suggested to be 3.0. The proposed spectra can almost envelop the average curves of time-history analysis results and are acceptable for utilization in shaking table tests of NSCs.

3) The developed FRS are adopted in shaking table tests of floating-type medical infusion racks to investigate their seismic response, and the corresponding seismic fragility curves are established based on the test results. These results indicate that the medical infusion racks exhibit a 50% probability of reaching or exceeding a residual displacement of 500 mm under 0.304 7g inputs when the proposed spectra are adopted for determining the shaking table input. The effectiveness and utilization of the proposed response spectra are demonstrated through a comparison of the results of shaking table tests with other response spectra.

4) For applying the newly developed FRS to different structure types, such as masonry and shear wall structures, further investigations are required. The developed floor response spectra will be used for performing seismic performance tests of different NSC types, investigating the seismic damage, and generating seismic fragility models to provide fundamental data for seismic performance evaluation and resilience assessment of buildings. Only then the applicability and effectiveness of the proposed FRS can be validated.

References

[1] Ministry of Housing and Urban-Rural Development of the People's Republic of China, General Administration of Quality Supervision, Inspection and Quarantine of the People's Republic of China. Code for seismic design of buildings: GB 50011—2010[S]. Beijing: China Architecture and Building Press, 2016. (in Chinese)

[2] Taghavi S, Miranda E. Response assessment of nonstructural building elements[R]. Berkeley, CA, USA: Pacific Earthquake Engineering Research Center, 2003.

[3] Wang Y M, Xiong L H, Xu W X. Seismic damage and damage enlightenment of medical buildings in Lushan M_s7.0 earthquake[J]. *Journal of Earthquake Engineering and Engineering Vibration*, 2013, **33**(4): 44 − 53. DOI: 10.11810/1000-1301.20130406. (in Chinese)

[4] Xie Y S, Xu Z D, Wang H. Occupant comfort evaluation of high-rise building under wind loads using LES[J]. *Journal of Southeast University* (*English Edition*), 2023, **39**(2): 127 − 132. DOI: 10.3969/j.issn.1003-7985.2023.02.003.

[5] Li Z Z, Chang X Y, Wang H, et al. Back-analysis method of rock mass properties in tunnel engineering using multiple monitoring data based on LS-SVR algorithm[J]. *Journal of Southeast University* (*English Edition*), 2023, **39**(1): 1 − 7. DOI: 10.3969/j.issn.1003-7985.2023.01.001.

[6] Xu L J, Xie L L. Bi-normalized response spectra and scalar periods for developing uniform seismic design spectra [J]. *Journal of Southeast University* (*English Edition*), 2007, **23**(2): 266 − 271.

[7] Lu G Y, Wang K H, Zhang P P. Performance-based system seismic assessment for long-span suspension bridges under two-level seismic hazard [J]. *Journal of Southeast University* (*English Edition*), 2019, **35**(4): 464 − 475. DOI: 10.3969/j.issn.1003-7985.2019.04.009.

[8] Zhu J C, Xiong L J. Experimental study on seismic behaviors of RC pier columns under different loading paths [J]. *Journal of Southeast University* (*Natural Science Edition*), 2020, **50**(6): 1006 − 1013. DOI: 10.3969/j.issn.1001-0505.2020.06.003. (in Chinese)

[9] Xu W J, Chen C, Chen M H, et al. Application of regression method in uncertainty analysis for numerical substructure in real-time hybrid simulation[J]. *Journal of Southeast University* (*Natural Science Edition*), 2020, **50**(1): 96 − 100. DOI: 10.3969/j.issn.1001-0505.2020.01.013. (in Chinese)

[10] Shang Q X, Zheng J Y, Li J C, et al. Comparative study of relevant specifications on peak floor acceleration in current codes of different countries[J]. *Engineering Mechanics*, 2020, **37**(S1): 91 − 96. DOI: 10.6052/j.issn.1000-4750.2019.05.S013. (in Chinese)

[11] Han Q H, Zhao Y F, Lu Y. Seismic behavior and resilience improvements of nonstructural components in the large public buildings—a review[J]. *China Civil Engineering Journal*, 2020, **53**(12): 1 − 10. DOI: 10.15951/j.tmgcxb.2020.12.001. (in Chinese)

[12] He S W, Qu Z, Zhou H M, et al. State of the art of testing methods for nonstructural components in seismic areas [J]. *China Civil Engineering Journal*, 2017, **50**(9): 16 − 27. DOI: 10.15951/j.tmgcxb.2017.09.003. (in Chinese)

[13] Shang Q X, Li J C, Wang T. State of the art of study on seismic performance of piping system[J]. *World Earth-*

quake Engineering, 2018, **34**(4): 174 − 181. (in Chinese)

[14] International Code Council Evaluation Service. Acceptance criteria for seismic qualification by shake-table testing of nonstructural components and systems: ICC-ES AC156 [S]. Whittier, CA, USA: International Code Council (ICC), 2006.

[15] Institute of Electrical and Electronics Engineers, Power Engineering Society. IEEE Recommended practice for seismic design of substations: IEEE Std 693-2005 [S]. New York, USA: IEEE Power Engineering Society, 2005.

[16] Ministry of Housing and Urban-Rural Development of the People's Republic of China, General Administration of Quality Supervision, Inspection and Quarantine of the People's Republic of China. Standard for aseismatic appraisal of electrical facilities in industrial plants: GB 50994—2014[S]. Beijing: China Planning Press, 2014. (in Chinese)

[17] Information industry of the People's Republic of China. Specification for seismic test of telecommunications equipment: YD 5083—2005 [S]. Beijing: Beijing University of Posts and Telecommunications Press, 2006. (in Chinese)

[18] Di Sarno L, Magliulo G, D'Angela D, et al. Experimental assessment of the seismic performance of hospital cabinets using shake table testing[J]. *Earthquake Engineering & Structural Dynamics*, 2019, **48**(1): 103 − 123. DOI: 10.1002/eqe.3127.

[19] Kuo K C, Suzuki Y, Katsuragi S, et al. Shake table tests on clutter levels of typical medicine shelves and contents subjected to earthquakes [J]. *Earthquake Engineering & Structural Dynamics*, 2011, **40**(12): 1367 − 1386. DOI: 10.1002/eqe.1094.

[20] Huang B F, Hua X, Lu W S. Seismic response behavior and shaking table tests on freestanding vase[J]. *Engineering Mechanics*, 2020, **37**(8): 112 − 122. DOI: 10.6052/j.issn.1000-4750.2019.09.0536. (in Chinese)

[21] Shang Q X. *Seismic performance study and fragility analysis of pipeline system*[D]. Harbin: Institute of Engineering Mechanics, China Earthquake Administration, 2018. (in Chinese)

[22] Bai W, Dai J W, Zhou H M, et al. Application of multiple tuned mass dampers on seismic protection of porcelain cylindrical electrical equipment [J]. *High Voltage Engineering*, 2018, **44**(3): 841 − 848. DOI: 10.13336/j.1003-6520.hve.20180301023. (in Chinese)

[23] Gong T. *Study on seismic design method of frame structures with rocking walls*[D]. Harbin: Institute of Engineering Mechanics, China Earthquake Administration, 2015. (in Chinese)

[24] Qu Z, Gong T, Li Q Q, et al. Evaluation of the fishbone model in simulating the seismic response of multistory reinforced concrete moment-resisting frames [J]. *Earthquake Engineering and Engineering Vibration*, 2019, **18**(2): 315 − 330. DOI: 10.1007/s11803-019-0506-9.

[25] Huang B F, Hua X, Lu W S, et al. Floor acceleration amplification factor in the instrumented buildings under historical earthquake excitations[J]. *China Civil Engineering Journal*, 2020, **53**(8): 16 − 27. DOI: 10.15951/j.tmgcxb.2020.08.002. (in Chinese)

[26] Shang Q X, Li J C, Wang T. Floor acceleration response spectra of elastic reinforced concrete frames[J]. *Journal of Building Engineering*, 2022, **45**: 103558. DOI: 10.1016/j.jobe.2021.103558.

[27] Wang T, Shang Q X, Li J C. Seismic force demands on acceleration-sensitive nonstructural components: A state-of-the-art review [J]. *Earthquake Engineering and Engineering Vibration*, 2021, **20**(1): 39 − 62. DOI: 10.1007/s11803-021-2004-0.

[28] Toro G R, McGuire R K, Cornell C A, et al. Linear and nonlinear response of structures and equipment to California and eastern United States earthquakes[R]. Palo Alto, CA, USA: Electric Power Research Institute, 1989.

[29] Welch D P. *Non-structural element considerations for contemporary performance-based earthquake engineering* [D]. Pavia, Italy: University of Pavia, 2016.

[30] Ministry of Housing and Urban-Rural Development of the People's Republic of China, General Administration of Quality Supervision, Inspection and Quarantine of the People's Republic of China. Code for seismic design of mechanical and electrical equipment: GB 50981—2014 [S]. Beijing: China Architecture and Building Press, 2014. (in Chinese)

[31] Ministry of Housing and Urban-Rural Development of the People's Republic of China. Code for seismic design of non-structural components: JGJ 339—2015[S]. Beijing: China Architecture and Building Press, 2015. (in Chinese)

[32] American Society of Civil Engineers. Minimum design loads for buildings and other structures: ASCE/SEI 7-16 [S]. Reston, VA, USA: American Society of Civil Engineers, 2016.

[33] Council of Standards New Zealand. Structural design actions. Part 5: Earthquake actions—New Zealand: NZS 1170.5: 2004[S]. Wellington, New Zealand: Council of Standards New Zealand, 2004.

[34] China Association for Engineering Construction Standardization. General rule for performance-based seismic design of buildings: CECS 160—2004[S]. Beijing: China Planning Press, 2004. (in Chinese)

[35] Federal Emergency Management Agency of the U.S. Department of Homeland Security. NEHRP recommended seismic provisions for new buildings and other structures: FEMA P-750 [R]. Washington DC, USA: Federal Emergency Management Agency, 2009.

[36] European Committee for Standardization. Eurocode 8 Design of structures for earthquake resistance-Part 1: General rules, seismic actions and rules for buildings: BS EN 1998-1:2004[S]. Brussels, Belgium: Commission of the European communities, European committee for Standardization, 2004.

[37] Anajafi H. *Improved seismic design of non-structural components (NSCs) and development of innovative control approaches to enhance the seismic performance of buildings and NSCs*[D]. Durham, NH, USA: University of New Hampshire, 2018.

[38] Tavares D H, Padgett J E, Paultre P. Fragility curves of typical as-built highway bridges in eastern Canada [J]. *Engineering Structures*, 2012, **40**: 107 − 118. DOI: 10.

1016/j. engstruct. 2012. 02. 019.
[39] Porter K, Kennedy R, Bachman R. Creating fragility functions for performance-based earthquake engineering [J]. *Earthquake Spectra*, 2007, **23**(2): 471 - 489. DOI: 10. 1193/1. 2720892.
[40] Nikfar F, Konstantinidis D. Shake table investigation on the seismic performance of hospital equipment supported on wheels/casters[J]. *Earthquake Engineering & Structural Dynamics*, 2017, **46**(2): 243 - 266. DOI: 10. 1002/eqe. 2789.

非结构构件抗震性能检测楼层反应谱

尚庆学[1,2,3] 李海洋[2,3] 李吉超[2,3] 王 涛[2,3]

([1] 中国地震灾害防御中心, 北京 100029)
([2] 中国地震局工程力学研究所地震工程与工程振动重点实验室, 哈尔滨 150080)
([3] 地震灾害防治应急管理部重点实验室, 哈尔滨 150080)

摘要:为了确定加速度敏感型非结构构件振动台试验的输入,建立了用于非结构构件抗震性能检测的楼层反应谱,并开展了浮放输液架振动台试验验证该楼层反应谱的可用性. 通过标准框架结构在不同地震强度下的弹塑性时程分析,确定非结构构件动力放大系数,基于分析结果建立了用于非结构构件抗震性能检测的楼层反应谱. 利用该反应谱及其他现有检测楼层反应谱进行了浮放输液架的振动台试验,基于试验结果建立了不同输入下非结构构件的地震易损性曲线. 提出的反应谱包括短周期段、上升段、平台段及下降段,平台段动力放大系数建议取值为 3.0. 试验结果表明,浮放输液架在 0.307 4g 的加速度输入下,即有 50% 的概率达到或超过 500 mm 的残余位移. 提出的楼层反应谱可为振动台试验确定台面输入,用于非结构构件抗震性能检测,促进加速度敏感型非结构构件的抗震性能研究.

关键词:非结构构件;楼层反应谱;振动台试验;抗震性能检测;易损性曲线
中图分类号:TU352. 1;TU317. 1